Singular Features of Large Fluctuations in Oscillating Chemical Systems†

M. I. Dykman,*,†,‡ V. N. Smelyanskiy,‡ R. S. Maier,§ and M. Silverstein‡

Department of Physics and Astronomy, Michigan State University, East Lansing, Michigan 48824, and Department of Mathematics, University of Arizona, Tucson, Arizona 85721

Received: September 10, 1996; In Final Form: October 10, 1996⊗

We investigate the way in which large fluctuations in an oscillating, spatially homogeneous chemical system take place. Starting from a master equation, we study both the stationary probability density of such a system far from its limit cycle and the optimal (most probable) fluctuational paths in its space of species concentrations. The flow field of optimal fluctuational paths may contain singularities, such as switching lines. A "switching line" separates regions in the space of species concentrations that are reached, with high probability, along topologically different sorts of fluctuational paths. If an unstable focus lies inside the limit cycle, the pattern of optimal fluctuational paths is singular and *self-similar* near the unstable focus. In fact, a switching line spirals down to the focus. The logarithm of the stationary probability density has a self-similar singular structure near the focus as well. For a homogeneous Selkov model, we provide a numerical analysis of the pattern of optimal fluctuational paths and compare it with analytic results.

I. Introduction

Chemical systems with ingoing and outgoing flows are an important class of nonequilibrium systems. For steady external conditions they can display unusual behavior of various sorts, including the presence of multiple stable stationary states and states of persistent oscillation (limit cycles in a space of species concentrations). These and other phenomena have been observed for autocatalysis in continuous flow stirred tank reactors.[1,2]

In many-particle systems, fluctuations about stable states are mostly small. For example, fluctuations in the number of molecules of a specified species are proportional to the square root of the mean number of molecules. However, large fluctuations also occasionally occur. Large fluctuations are responsible for transitions between coexisting stable states of a system. They are of particular interest for mesoscopic systems, including biochemical systems where it has been noticed[3,4] that the average number of molecules of a species in a vesicle may differ substantially from an estimate based on the density of the species in the surrounding solution.

If stirring is sufficiently rapid, the reacting system is spatially uniform, and the only dynamical variables are the total number of molecules of each species, $\mathbf{X} \equiv (X_1, X_2, ...)$. In systems with limit cycles these numbers depend periodically on time, if fluctuations are neglected. Because of the explicitly broken time symmetry, fluctuations in such oscillating systems are qualitatively different from fluctuations in systems in thermal equilibrium. An analysis of fluctuations around a limit cycle was recently performed, in both stationary and transient regimes (see ref 5 and references therein). In the present paper we investigate large fluctuations away from a limit cycle.

A fluctuation to the vicinity of a given state $\mathbf{X}$ may occur in many ways. However, the probability densities for different fluctuational trajectories $\mathbf{X}(t)$ are different, and for large fluctuations the probability density in "trajectory space" peaks sharply (indeed exponentially sharply) at a single most probable path $\mathbf{X}_{opt}(t)$ extending from the limit cycle to $\mathbf{X}$. Such optimal (i.e., most probable) fluctuational paths are physically real. In fact, for fluctuating continuous dynamical systems they have been observed experimentally.[6]

In Markovian systems in thermal equilibrium, optimal fluctuational trajectories are time-reversed deterministic trajectories (cf. ref 2; see also ref 7). This is not the case in nonequilibrium systems, in general. It was found numerically for fluctuating dynamical systems[8−10] and for chemical systems[11] that the pattern of optimal paths may have singularities even in the case when the deterministic paths are smooth. These singularities are similar to those seen in the pattern of extreme paths, when one computes a semiclassical (WKB) approximation to a quantum-mechanical wave function.[12] However, there is a fundamental difference between optimal fluctuational paths and the extreme paths of WKB theory: optimal paths determine a real and positive probability density and may be directly observed, whereas extreme paths determine the phase of a wave function and, at most, the shape of an interference pattern. Therefore we may expect different types of singularities to occur in the pattern of optimal paths.

In this paper we consider a chemical oscillator of the simplest type, one with two species, and perform a global and local analysis of the pattern of optimal fluctuational paths emanating from its limit cycle in the (X_1, X_2)-plane. In section II we describe an eikonal approximation to the solution of its master equation, in the stationary regime. In section III we formulate a problem of Hamiltonian dynamics, whose solution will determine the optimal paths and give the logarithm of the stationary probability density. In section IV we discuss singular features of the pattern of optimal paths, by applying the results of catastrophe theory to the auxiliary Hamiltonian system. In section V we consider the case when the limit cycle contains an unstable focus. We linearize Hamilton's equations near this unstable focus and discuss the eigenvalues and eigenvectors of the resulting linear problem. Section VI is the central part of the paper, as in this section we show that generically the flow field of optimal paths is self-similar near the focus. In section VII we use our results to find the shape of the stationary probability distribution near the focus and the switching line that separates the areas in the (X_1, X_2)-plane to which the system fluctuates, with high probability, along topologically different

† This paper is dedicated to John Ross with deep respect and sincere gratitude.

‡ Michigan State University.

§ University of Arizona.

⊗ Abstract published in *Advance ACS Abstracts,* November 15, 1996.

S0022-3654(96)02746-3 CCC: $12.00

paths. In section VIII we numerically analyze large fluctuations in a spatially homogeneous Selkov model with a limit cycle. Section IX contains concluding remarks.

II. Eikonal Approximations in Chemical Kinetics

A. The Master Equation. For dilute homogeneous chemical systems, time intervals between reactions greatly exceed the reaction duration, and the probability of a reaction depends on the number of molecules only at a given instant of time. That is, there are no appreciable memory effects. Therefore the evolution of the probability density $P(\mathbf{X},t)$ of the vector $\mathbf{X} \equiv (X_1, X_2)$, whose components are the number of molecules of each species, is given by a Markovian master equation

$$\frac{\partial P(\mathbf{X},t)}{\partial t} = \sum_{\mathbf{r}} [W(\mathbf{X}-\mathbf{r},\mathbf{r})\, P(\mathbf{X}-\mathbf{r},t) - W(\mathbf{X},\mathbf{r})\, P(\mathbf{X},t)] \qquad (1)$$

Here $W(\mathbf{X},\mathbf{r})$ is the probability per unit time for the transition $\mathbf{X} \rightarrow \mathbf{X} + \mathbf{r}$ to occur. The vector $\mathbf{r} \equiv (r_1, r_2)$ shows the change in the numbers of molecules in a reaction. The transition rates $W(\mathbf{X},\mathbf{r})$ are smooth functions of $\mathbf{X}$ (often they are polynomials in X_i[13,14]).

In a macroscopic (or mesoscopic) system the mean numbers of molecules are proportional to the volume Ω, as are the probabilities $W(\mathbf{X},\mathbf{r})$. We take Ω to be dimensionless and large, i.e., $\Omega \gg 1$. (In fact, Ω can be thought of as the mean total number of molecules.) It is convenient to introduce a vector $\mathbf{x}$ whose components are the density of each species and reduced transition probabilities $w(\mathbf{x},\mathbf{r})$:

$$\mathbf{x} \equiv \mathbf{X}/\Omega, \quad w(\mathbf{x},\mathbf{r}) \equiv W(\mathbf{X},\mathbf{r})/\Omega \qquad (2)$$

An evolution equation for the vector of *mean* densities $\bar{\mathbf{x}}(t)$, defined by

$$\bar{\mathbf{x}}(t) \equiv \Omega^{-1} \sum_{\mathbf{X}} \mathbf{X} P(\mathbf{X},t) \qquad (3)$$

can be obtained from (1) to zeroth order in Ω^{-1}. It is known[13] to be of the form

$$\frac{\mathrm{d}\bar{\mathbf{x}}}{\mathrm{d}t} = \sum_{\mathbf{r}} \mathbf{r} w(\bar{\mathbf{x}},\mathbf{r}) \qquad (4)$$

We shall consider the case when the stable stationary solution of (4) is a limit cycle $\bar{\mathbf{x}}^{(\mathrm{cl})}(t)$, with a period $\tau^{(\mathrm{cl})}$. That is,

$$\bar{\mathbf{x}}^{(\mathrm{cl})}(t) = \bar{\mathbf{x}}^{(\mathrm{cl})}(t+\tau^{(\mathrm{cl})}) \qquad (5)$$

The reacting system with specified initial densities (x_1, x_2) will approach the limit cycle (5) over a relaxation time t_r and then move along the limit cycle. However, because of the number of molecules being finite, fluctuations away from the limit cycle will occur. In fact, a steady-state probability distribution will be formed.

The evolution of the probability density $P(\mathbf{X},t)$ close to the cycle was analyzed in ref 5. Over a period of time proportional to Ω phase diffusion occurs: the "chemical clocks" become mistuned. It is this that causes a stationary density P_{st} to be formed; as $t \rightarrow \infty$, $P(\mathbf{X},t) \rightarrow P_{\mathrm{st}}(\mathbf{x})$. (For a different source of fluctuations, this effect is well-known for lasers and ac generators, cf. ref 15). The steady-state density $P_{\mathrm{st}}(\mathbf{x})$ satisfies the equation

$$\sum_{\mathbf{r}} [w(\mathbf{x}-\Omega^{-1}\mathbf{r})\, P_{\mathrm{st}}(\mathbf{x}-\Omega^{-1}\mathbf{r}) - w(\mathbf{x})\, P_{\mathrm{st}}(\mathbf{x})] = 0 \qquad (6)$$

The function $P_{\mathrm{st}}(\mathbf{x})$ is crater shaped,[16] with a maximum on the cycle (see ref 17 for the shape of the distribution when the reacting system is close to a Hopf bifurcation point). The width of the distribution in the direction normal to the cycle is proportional to $\Omega^{-1/2}$.

B. The Eikonal Approximation. The stationary probability density $P_{\mathrm{st}}(\mathbf{x})$, in the limit $\Omega \gg 1$, may most easily be analyzed by means of an *eikonal approximation*. This approximation has much in common with the WKB approximation in quantum mechanics.[12] The role of $\hbar$ is played by Ω^{-1}.

The idea behind the eikonal approximation is that the density $P_{\mathrm{st}}(\mathbf{x})$ is a much steeper function of $\mathbf{x}$ than the coefficients $w(\mathbf{x},\mathbf{r})$. (Similarly, a rapidly oscillating semiclassical wave function is a much steeper function of the coordinates than the potential in the Schrödinger equation that it satisfies.) Indeed, it follows from eqs 7 and 8 below that in general, $P_{\mathrm{st}}(\mathbf{x})$ varies on a characteristic length scale of order Ω^{-1}. On the other hand, the coefficients $w(\mathbf{x},\mathbf{r})$ vary only slightly when $\mathbf{x}$ is changed by Ω^{-1}.

In the limit of large Ω we seek a solution of eq 6 that is of eikonal form, i.e.,

$$P_{\mathrm{st}}(\mathbf{x}) \approx c(\mathbf{x}) \exp[-\Omega S(\mathbf{x})] \qquad (7)$$

(cf. ref 18). Here S is an eikonal function, and c is a slowly varying "prefactor" function whose properties we shall not explore in this paper in any detail. Instead, we shall focus on S. Substituting (7) into (6), and keeping only the terms of lowest order in Ω^{-1}, yields the following equation for the function S:

$$H(\mathbf{x},\partial S(\mathbf{x})/\partial \mathbf{x}) = 0, \quad H(\mathbf{x},\mathbf{p}) \equiv \sum_{\mathbf{r}} w(\mathbf{x},\mathbf{r})[\exp(\mathbf{r}\cdot\mathbf{p}) - 1] \qquad (8)$$

Equation 8 is a nonlinear first-order partial differential equation for the eikonal function $S(\mathbf{x})$. A similar equation arises in the asymptotic analysis of Markov chains[19] and Markov jump processes.[20] In the context of chemical kinetics, eq 8 was considered in refs 11 and 21 (in ref 11, large fluctuations in homogeneous chemical systems with point attractors were analyzed).

C. The Distribution near the Limit Cycle. Equation 8 can be solved near the limit cycle. To approximate the function S there, it is convenient to introduce local coordinates ξ_1 and ξ_2 such that the corresponding unit vectors $\boldsymbol{\xi}_1$ and $\boldsymbol{\xi}_2$ are locally parallel and perpendicular to the limit cycle, respectively. The coordinate ξ_1 is the distance along the cycle (measured from an arbitrary point on the cycle), and we have

$$\boldsymbol{\xi}_1 = \sum_{\mathbf{r}} \mathbf{r} w(\bar{\mathbf{x}}^{(\mathrm{cl})},\mathbf{r})/v \qquad (9)$$

where

$$v = v(\xi_1) \equiv |\sum_{\mathbf{r}} \mathbf{r} w(\bar{\mathbf{x}}^{(\mathrm{cl})},\mathbf{r})| \qquad (10)$$

Here $v(\xi_1)$ is the (position-dependent) velocity of the system on the cycle, in the absence of fluctuations. We set $\xi_2 = 0$ on the cycle. At any point on the cycle, the matrix of partial derivatives $(\partial x_i/\partial \xi_j)$ of the transformation from the old to the new variables is orthogonal.

Since the stationary density $P_{\mathrm{st}}(\mathbf{x})$ has a maximum on the cycle, the function S has a minimum in the ξ_2-direction at $\xi_2 = 0$. Therefore the derivative

$$\partial S/\partial \xi_2 = 0 \quad \text{at} \quad \xi_2 = 0$$

and a Taylor series for S will start with the term that is quadratic

in ξ_2. It is not difficult to deduce from eq (8) that $\partial S/\partial\xi_1$ must also equal zero at $\xi_2 = 0$, i.e.,

$$[S(\mathbf{x})]_{\xi_2=0} = \text{const}$$

In what follows, we choose a normalization by setting this constant equal to zero. Accordingly near the limit cycle

$$S(\mathbf{x}) \approx {}^1/_2\lambda(\xi_1)\xi_2^2, \quad |\xi_2| \ll 1 \tag{11}$$

The function $\lambda(\xi_1)$ gives the curvature of the function S in the direction normal to the cycle.

To find the function λ, one should substitute (11) into (8), and expand $w(\mathbf{x},\mathbf{r})$ in eq 8 about $\bar{\mathbf{x}}^{(\mathrm{cl})}$ to first order in ξ_2. This gives a first-order differential equation for λ, which must be solved with the boundary condition of periodicity of S (and thus of λ) on the cycle, i.e.,

$$\lambda(\xi_1+l^{(\mathrm{cl})}) = \lambda(\xi_1)$$

where $l^{(\mathrm{cl})}$ is the length of the cycle. The corresponding solution is of the form (cf. ref 16; see also refs 22, 23)

$$\lambda^{-1}(\xi_1) = \int_0^{\xi_1} v^{-1}(y)\,\mathrm{d}y\; Q^{(\mathrm{cl})}(y)\;\rho(\xi_1,y) + \frac{\rho(\xi_1,0)}{1-\rho(l^{(\mathrm{cl})},0)}\int_0^{l^{(\mathrm{cl})}}\mathrm{d}x\; v^{-1}(y)\;Q^{(\mathrm{cl})}(y)\;\rho(l^{(\mathrm{cl})},y) \tag{12}$$

where

$$\rho(x,x') \equiv [-2\int_{x'}^{x}\mathrm{d}\xi_1\;\zeta(\xi_1)], \quad Q^{(\mathrm{cl})}(\xi_1) \equiv \sum_{\mathbf{r}}(\mathbf{r}\cdot\boldsymbol{\xi}_2)^2\; w(\mathbf{x}^{(\mathrm{cl})},\mathbf{r}) \tag{13}$$

with

$$\zeta(\xi_1) \equiv -v^{-1}(\xi_1)\sum_{\mathbf{r}}(\mathbf{r}\cdot\boldsymbol{\xi}_2)[\partial w(\mathbf{x},\mathbf{r})/\partial\xi_2]_{\xi_2=0} \tag{14}$$

It is not difficult to see that $\lambda(\xi_1) > 0$ for all ξ_1. This is a consequence of the inequality

$$\int_0^{l^{(\mathrm{cl})}}\mathrm{d}\xi_1\zeta(\xi_1) > 0$$

which is a criterion for the stability of the cycle in the absence of fluctuations.

The stationary probability density $P_{\mathrm{st}}(\mathbf{x})$ as given by eqs 7 and 11 is Gaussian in the transverse coordinate ξ_2. In fact λ is a position-dependent reciprocal variance. Equations 7 and 11 apply up to the not too far tail of the distribution $P_{\mathrm{st}}(\mathbf{x})$, where $\lambda\xi_2^2 \gg \Omega^{-1}$ but $\xi_2^2 \ll 1$. For larger $|\xi_2|$ the distribution will be non-Gaussian, and to find it, one would have to use eq 7 without approximating S.

We note in passing that the prefactor of the transverse Gaussian distribution, like the reciprocal variance λ, depends on ξ_1, the position along the limit cycle. It was given in ref 16; see also ref 23.

III. Extreme Fluctuational Trajectories

A. Equations for the Extreme Trajectories. The analysis of section II does not apply far from the limit cycle. A convenient way to analyze the function $S(\mathbf{x})$ over a broad range of species concentrations $\mathbf{x}$ is based on the idea that eq 8 can be viewed as a Hamilton−Jacobi equation for an auxiliary classical-mechanical system, with Hamiltonian function $H(\mathbf{x},\mathbf{p})$. In this interpretation, $\mathbf{p}$ is a momentum variable, and the eikonal function S is a *classical action at zero energy*. This idea was first used to analyze fluctuation phenomena in continuous Markov systems.[24]

Hamilton's equations of motion for the dynamical system with the Hamiltonian of (8) are of the standard form:[25]

$$\dot{\mathbf{x}} = \sum_{\mathbf{r}}\mathbf{r}w(\mathbf{x},\mathbf{r})\,\exp(\mathbf{r}\cdot\mathbf{p})$$

$$\dot{\mathbf{p}} = -\sum_{\mathbf{r}}[\exp(\mathbf{r}\cdot\mathbf{p}) - 1]\frac{\partial w(\mathbf{x},\mathbf{r})}{\partial\mathbf{x}} \tag{15}$$

They determine classical trajectories in a four-dimensional phase space of the auxiliary system, whose coordinates and momenta are the 2-vectors $\mathbf{x}$ and $\mathbf{p}$. Along any zero-energy classical trajectory, S will satisfy the differential equation

$$\dot{S} = L(\mathbf{x},\dot{\mathbf{x}}) \tag{16}$$

Here $L(\mathbf{x},\dot{\mathbf{x}})$ is the Lagrangian corresponding to the Hamiltonian H, i.e.,

$$L(\mathbf{x},\dot{\mathbf{x}}) = \mathbf{p}\dot{\mathbf{x}} - H(\mathbf{x},\mathbf{p}) \tag{17}$$

The differential equation (16) may be integrated numerically, in tandem with Hamilton's equations, to yield the value of S at points lying along any zero-energy trajectory. We shall call such trajectories "extreme trajectories", since any such trajectory will be an extremum of the action functional

$$S[\mathbf{x}(t)] \equiv \int_{t_{\min}}^{t_{\max}}L(\mathbf{x}(t),\dot{\mathbf{x}}(t))\,\mathrm{d}t \tag{18}$$

though possibly not a minimum. The quantity $S(\mathbf{x})$ appearing in the eikonal approximation (7) is really a *minimum* classical action at zero energy. Numerical computation of $S(\mathbf{x})$ requires a minimization over all extreme trajectories terminating at $\mathbf{x}$.

The physical meaning of the extreme trajectories and the initial conditions for eqs 15 follow from a now standard picture of the way in which large fluctuations occur.[6,24,26,27] The stationary density at a point $\mathbf{x}$ far from the limit cycle is formed by occasional large fluctuations. The value of $P_{\mathrm{st}}(\mathbf{x})$ is determined, to logarithmic accuracy as $\Omega \to \infty$, by the frequency with which the *most probable*, or *optimal*, fluctuation to the point $\mathbf{x}$ occurs. The optimal fluctuational trajectory $\mathbf{x}_{\mathrm{opt}}(t)$ along which the system must move in order to reach $\mathbf{x}$ is a particular extreme trajectory: the least-action one that terminates at $\mathbf{x}$. One way to see this is based on the path-integral formulation of fluctuation theory; for systems described by master equations such a formulation was developed in ref 18. In this formulation, extreme trajectories are extrema of the path-integral expression for a transition probability.

The preceding picture, involving an extremum of an action or action-like functional, is similar to the theoretical infrastructure of the WKB approximation used in the $\hbar \to 0$ limit of quantum mechanics.[12] Both in the semiclassical limit of quantum mechanics and in the problem of large fluctuations as $\Omega \to \infty$, there may be several extreme paths $\mathbf{x}(t)$ that terminate at the same point $\mathbf{x}$. In the semiclassical limit of quantum mechanics all extreme paths are "meaningful": if the action $S(\mathbf{x})$ is multivalued, the wave function will be a sum of terms proportional to the several values of $\exp(\mathrm{i}S(\mathbf{x})/\hbar)$. In contrast, in the present problem the stationary probability density would be a sum of terms proportional to the several values of $\exp(-\Omega S(\mathbf{x}))$. The absence of an "i" in the exponent explains why only the least-action extreme path is physically meaningful; as $\Omega \to \infty$, it dominates all others.

Optimal fluctuational trajectories and other extreme trajectories start in the vicinity of the limit cycle, where the system

spends most of its time. In fact they emerge from the limit cycle at $t = -\infty$, and gradually move away. On the cycle the action is constant (cf. ref 11), and $\mathbf{p} = \partial S/\partial \mathbf{x} = \mathbf{0}$. Therefore the initial conditions for eqs 15 are of the form

$$\mathbf{x}(t) \sim \mathbf{x}^{(\mathrm{cl})}(t), \quad \mathbf{p}(t) \to 0, \quad S(t) \to 0 \quad \text{as} \quad t \to -\infty \tag{19}$$

B. Extreme Trajectories near the Limit Cycle. To find the flow of outgoing extreme trajectories as they emerge from the limit cycle, it is convenient to change eqs 15 to the coordinates (ξ_1, ξ_2) discussed in section IIC. Since $\mathbf{p} = \partial S/\partial \mathbf{x}$, the quadratic approximation (11) to the action implies

$$\mathbf{p} \approx \lambda(\xi_1)\xi_2 \boldsymbol{\xi}_2 \qquad \xi_2 \to 0 \tag{20}$$

Linearizing eqs 15 in ξ_2, the distance from the cycle, and using (20), we obtain

$$\xi_1(t) = \xi_1(t_0) + \int_{t_0}^{t} \nu \, \mathrm{d}\tau \tag{21}$$

$$\frac{\xi_2(t)}{\xi_2(t_0)} = M(\xi_1(t),\xi_1(t_0))$$

where

$$M(\xi_1,\xi_1') = \left[\frac{\lambda(\xi_1')}{\lambda(\xi_1)}\right]^{1/2} \exp\left\{\frac{1}{2}\int_{\xi_1'}^{\xi_1} \mathrm{d}y[\lambda(y)\, Q^{(\mathrm{cl})}(y)\, \nu^{-1}(y)]\right\} \tag{22}$$

Since $\lambda = \lambda(\xi_1)$ is a periodic function, and $\lambda > 0$, $Q^{(\mathrm{cl})} > 0$, it follows from (21) that the extreme trajectories spiral away from the limit cycle. The distance from the cycle is increased over each turn by a factor

$$M \equiv M(\xi_1 + l^{(\mathrm{cl})}, \xi_1)$$

The direction of rotation is the same as that of the limit cycle.

One can see from eqs 20 and 21 that the flow of extreme trajectories is self-similar near the limit cycle. A path that goes through the point (ξ_1, ξ_2) goes also through the point $(\xi_1 + l^{(\mathrm{cl})}, M\xi_2)$. Since the values ξ_1 and $\xi_1 + l^{(\mathrm{cl})}$ are physically identical, this means that the entire flow of the outgoing extreme trajectories may be mapped onto two intervals of ξ_2, one for positive and one for negative ξ_2, which lie between the neighboring turns of two extreme trajectories on opposite sides of the cycle. In other words, outgoing trajectories form a one-parameter set $\mathbf{x}(t;\xi_2^{(0)})$, $\mathbf{p}(t;\xi_2^{(0)})$, with the parameter $\xi_2^{(0)}$ lying within an interval between μ and $M\mu$, with $|\mu| \ll 1$ but otherwise arbitrary. Instead of using (19), we may accordingly set initial conditions for the outgoing extreme trajectories at a finite time t_0:

$$\mathbf{p}(t_0,\mu) = \lambda(\xi_1(t_0))\mu\boldsymbol{\xi}_2, \quad \mathbf{x}(t_0,\mu) = \bar{\mathbf{x}}^{(\mathrm{cl})}(t_0) + \mu\boldsymbol{\xi}_2, \quad S(t_0,\mu) = {}^1\!/_2\lambda(\xi_1(t_0))\mu^2 \tag{23}$$

Clearly, $\xi_1(t_0) \equiv |\bar{\mathbf{x}}^{(\mathrm{cl})}(t_0)|$, and $\xi_2(t_0) \equiv \mu$. By integrating Hamilton's equations, equipped with these initial conditions, forward in time, we can in effect coordinatize the space of species concentrations near the limit cycle by μ (which labels the outgoing extreme trajectories) and t (the transit time along any given extreme trajectory).

Equations 15 and 23 make it possible to perform a numerical analysis of the set of extreme trajectories $\mathbf{x}(t,\mu)$, $\mathbf{p}(t,\mu)$ and the corresponding action function $S(t,\mu)$. The results of such an analysis will be given in section VIII. We emphasize to the reader that even though the present formulation seems remote from the original reacting chemical system, it will yield $S(\mathbf{x})$: the value of the eikonal function at any specified vector of species concentrations $\mathbf{x}$. This in turn will yield an approximation to the value of the stationary probability density at the point $\mathbf{x}$ in the species concentration space.

IV. Singular Features of the Pattern of Extreme Paths

As we noted above, although extreme trajectories $(\mathbf{x}(t,\mu), \mathbf{p}(t,\mu))$ with different values of the parameter μ do not intersect each other in the four-dimensional phase space, trajectories $\mathbf{x}(t,\mu)$ with different values of the parameter μ may pass through the same point $\mathbf{x}$. For these trajectories the values of the action $S(t,\mu)$ are different; that is, the action $S(\mathbf{x})$ is a multivalued function of $\mathbf{x}$. The surface of *minimum* action $S_{\min} = S_{\min}(\mathbf{x})$ can be constructed piecewise from the lowest sheets of the surface $S = S(\mathbf{x})$.

Generically, the surface $S_{\min} = S_{\min}(\mathbf{x})$ has singular curves along which different sheets of the surface $S = S(\mathbf{x})$ intersect each other. On these curves the first derivative of $S_{\min}(\mathbf{x})$ in the transverse direction is discontinuous.[8,28] The global structure of $S_{\min} = S_{\min}(\mathbf{x})$ and related singular features of the pattern of optimal trajectories can be understood from an analysis of the generic topological properties of the auxiliary Hamiltonian system in its four-dimensional phase space. For noise-driven dynamical systems such an analysis was carried out in ref 29. We show below that the results apply to systems described by master equations as well.

In the four-dimensional phase space of the auxiliary system, the limit cycle of the original reacting chemical system can be viewed as lying in the plane $\mathbf{p} = 0$. That is, this plane is the plane of species concentrations (x_1, x_2). The extreme trajectories, which satisfy Hamilton's equations (15), emanate from the limit cycle and form a two-dimensional surface known as a Lagrangian manifold (LM).[30,31] The trajectories never intersect each other on the LM: only one trajectory goes through a given point $(\mathbf{x}, \mathbf{p})$. However, the LM may have a complicated structure in the phase space and in general will have singular projections onto the plane $\mathbf{p} = \mathbf{0}$.[30]

It was shown by Whitney[33] that, generically, a smooth surface may have only two types of singularities, namely, folds and cusp points from which folds emanate in pairs, as shown in Figure 1. If the LM formed by the trajectories $(\mathbf{x}(t,\mu), \mathbf{p}(t,\mu))$ has folds, then the projections of the folds of the LM onto the species concentration plane $\mathbf{p} = \mathbf{0}$ will be *caustics*. As shown in Figure 1, a caustic is the envelope of a family of paths of the form $\mathbf{x}(t,\mu)$. To put it another way, a caustic is a curve in the two-dimensional space of species concentrations from which extreme trajectories are *reflected*. Caustics may merge together at cusp points.

Extreme trajectories $\mathbf{x}(t,\mu)$ reflected from different caustics do not intersect each other unless there are other cusp points, since the paths $(\mathbf{x}(t,\mu), \mathbf{p}(t,\mu))$ lie on the same sheet of the LM (the middle sheet of the LM shown in Figure 1). Therefore the points inside the area bounded by the caustics can be reached along three different paths: two paths that have not yet touched a caustic and one that has been reflected from a caustic. Correspondingly, the action $S(\mathbf{x})$ takes on three values. Only the minimum value (the lowest branch of the multivalued function $S(\mathbf{x})$) is of physical interest, as we have explained.

We now show that the action computed from an extreme path that has been reflected from a caustic is larger than the action computed from an extreme path that has not. Near a caustic it

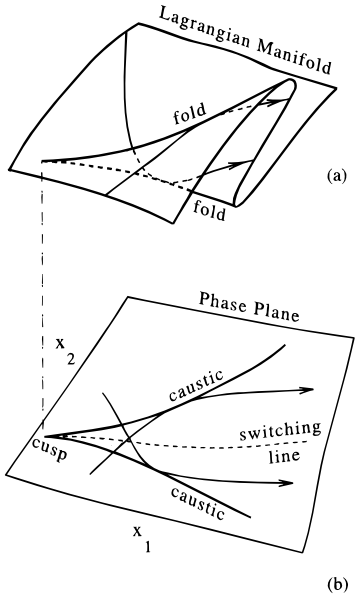

Figure 1. Singular feature of the sort that may appear in the flow field of extreme fluctuational trajectories. (a) The Lagrangian manifold formed by the zero-energy trajectories of the auxiliary Hamiltonian system, in its four-dimensional phase space. The manifold contains a fold, in fact, a joined pair of folds. (b) Extreme fluctuational trajectories, obtained by projecting these zero-energy trajectories down to the plane of species concentrations (x_1, x_2). The projections of the folds in the Lagrangian manifold are called *caustics*; the extreme trajectories are reflected from them. The caustics in part b emerge from a cusp point, which is the projection of the point where the folds join. A switching line, discussed further in the text, lies between the two caustics; it separates the regions in the space of species concentrations that are reached along different sorts of optimal fluctuational trajectories.

is convenient to choose coordinates so that $\hat{x}_1$ points along the caustic, and x_2 is the distance to the caustic. This implies that

$$\dot{\mathbf{x}} = \hat{\mathbf{x}}_1|\dot{\mathbf{x}}|, \quad \text{at } x_2 = 0$$

As shown in Figure 1, the coordinate x_2 is quadratic in the momentum component transverse to the caustic. So this momentum component has two branches, i.e.,

$$p_2^{\pm}(x_1,x_2) = p_2(x_1,0) \pm [A(x_1)x_2]^{1/2}, \quad |x_2| \ll 1 \qquad (24)$$

The sign of A determines whether the extreme trajectories that are reflected from the caustic lie on the $x_2 > 0$ side (for $A > 0$) or on the $x_2 < 0$ side (for $A < 0$).

The action $S(\mathbf{x})$ as a function of $\mathbf{x}$ also has two branches near the caustic. The quantity of interest is the difference between the values of S on its two sheets, at the same point $\mathbf{x}$. Since extreme trajectories are zero-energy classical trajectories, the action S as a function of (t,μ) is given by the integral

$$S(t,\mu) = \int \mathrm{d}t\, \mathbf{p}(t,\mu)\cdot\mathbf{x}(t,\mu) \qquad (25)$$

Therefore the difference between the values of S on the two sheets may be written as

$$S^{(+)}(\mathbf{x}) - S^{(-)}(\mathbf{x}) = \int_{x_2=0}^{x_2} p_2^{(+)}\, dx_2 - \int_{x_2=0}^{x_2} p_2^{(-)}\, \mathrm{d}x_2 \qquad (26)$$

It follows from the equations of motion (15), with account taken of (24) and of the fact that on the caustic the transverse velocity $\dot{x}_2$ is zero, that near the caustic

$$\dot{x}_2^{(\pm)} \approx \sum_{\mathbf{r}} r_2{}^2 w(\mathbf{x},\mathbf{r}) \exp[\mathbf{r}\cdot\mathbf{p}(x_1,0)][p_2^{(\pm)}(x_1,x_2) - p_2(x_1,0)] \qquad (27)$$

From this equation it follows that $\dot{x}_2 = \mathrm{sgn}[p_2^{(\pm)}(x_1,x_2) - p_2(x_1,0)]$. It follows then from eqs 24 and 26 that the smaller action corresponds to the trajectories that *approach* the caustic (for which $\dot{x}_2/x_2 < 0$), whereas the action for the trajectories that have been reflected from the caustic is larger, at the same point $\mathbf{x}$.

A. The Switching Line. The preceding argument shows that when the Lagrangian manifold of the auxiliary Hamiltonian system has a fold as shown in Figure 1, in which case $\mathbf{p} = \mathbf{p}(\mathbf{x})$ has three branches, the action associated with points $(\mathbf{x}, \mathbf{p})$ in phase space that lie on the "middle" sheet of the Lagrangian manifold will never be the minimum action. Equivalently, the least of the three values of $S(\mathbf{x})$, one value being associated with each sheet, must be attained on the top or bottom sheet of the Lagrangian manifold. The reason is that the middle sheet is formed by extreme trajectories that have "gone over a fold", i.e., have been reflected from a caustic. Such trajectories cannot have minimum action.

Let us label the upper and lower sheets of the Lagrangian manifold with the superscripts 1 and 2, respectively. The corresponding action sheets $S^{(1,2)} = S^{(1,2)}(\mathbf{x})$ intersect along a curve on the (x_1, x_2) plane, which is determined by the equation

$$S^{(1)}(\mathbf{x}) = S^{(2)}(\mathbf{x}) \qquad (28)$$

If the fold in the Lagrangian manifold merges with another fold at a cusp point, this curve will terminate there, since that is where the sheets $S^{(1,2)}$ merge. Moreover, this curve will lie between the two folds, i.e., between the two corresponding caustics (Figure 1b). Points that are a small distance away from this curve but lie on opposite sides of it are reached via topologically different optimal paths; these paths generate the actions $S^{(1)}$ and $S^{(2)}$, respectively. It is reasonable therefore to call the line determined by (28) a *switching line*. For noise-driven continuous dynamical systems the presence of a switching line has recently been observed experimentally.[6b]

The stationary probability density of the system will be regular in the vicinity of a switching line. Away from a cusp, but near the switching line, it will have the form (cf. refs 28b, 29)

$$P_{\mathrm{st}}(\mathbf{x}) \approx \sum_{i=1,2} c^{(i)}(\mathbf{x}) \exp[-\Omega S^{(i)}(\mathbf{x})], \quad \Omega \to \infty \qquad (29)$$

That is, both $S^{(1)}$ and $S^{(2)}$ will contribute. The prefactors $c^{(i)}$ in (17) are known to blow up as $\mathbf{x}$ approaches a cusp point. For continuous Markov systems, an explicit form for the prefactor in the vicinity of a cusp point was obtained in ref 29, and the form can easily be generalized to the present case.

Once an extreme trajectory crosses the switching line, by definition it no longer provides the minimum action. Well beyond the switching line (at a distance $\gg \Omega^{-1}$) it does not contribute significantly to the stationary probability density of the system. As is shown in Figure 1, if a fold is present, extreme trajectories cross the associated switching line *before* they are reflected from a caustic. As a consequence, caustics are never reached by optimal paths: by the time an optimal path reaches a caustic and is reflected from it, the path has ceased to be optimal. For this reason, caustics are "unobservable": the observable singular features of the flow field of optimal trajectories emanating from the limit cycle are, instead, switching lines and cusp points.

V. Extreme Trajectories near an Unstable Focus

Two-variable dynamical systems with a stable limit cycle have a dynamically unstable stationary state or an unstable limit cycle inside the stable cycle.[31] A simple and very general

situation is where this state is an unstable focus, the location of which we symbolize by $\mathbf{x}_f$. In the chemical kinetics context, the presence of a focus $\mathbf{x}_f$ in the space of species concentrations may be determined by examining the deterministic equations (4). If a focus is present, it gives rise to a fixed point $\mathbf{x} = \mathbf{x}_f$, $\mathbf{p} = \mathbf{0}$ of the auxiliary Hamiltonian system (8), and (15) in its four-dimensional phase space.

In the following sections we shall investigate the pattern of optimal fluctuational trajectories and the stationary probability density, in the vicinity of an unstable focus of a reacting two-component chemical system. We shall show that, except the case when the system is close to a Hopf bifurcation point and radial and angular fluctuations near the unstable focus are essentially independent of each other, the pattern of optimal trajectories is *singular*. Despite the completely different origin of fluctuations, the singularities of the pattern appear to be similar to those discussed in ref 32 for noise-driven continuous dynamical systems with a stable limit cycle. The results we shall obtain apply not only to systems with a stable limit cycle but to arbitrary systems with an unstable focus.

A. The Hamiltonian near the Unstable Focus. The unstable focus $\mathbf{x}_f$ is determined by the dynamical equations (4) for the mean species concentrations of the reacting chemical system and must satisfy the time-independent equation

$$\sum_{\mathbf{r}} \mathbf{r} w(\mathbf{x}_f, \mathbf{r}) \equiv 0 \tag{30}$$

We shall assume that at the focus $\Omega|\mathbf{x}_f| \gg 1$, and that eq 4 for the mean densities is meaningful. However, even if this is not true, the results below will still apply, since the structure we shall discover arises at distances from the focus $|\mathbf{x} - \mathbf{x}_f|$, which, though small compared to the length scale of the limit cycle, are much larger than $\Omega^{-1/2}$.

It follows from the inequality $e^z - z - 1 \geq 0$ and from the nonnegativity of the transition probabilities $w(\mathbf{x},\mathbf{r})$ that eqs 8 and 30 can be satisfied at the focus only if $\mathbf{p} = \mathbf{0}$ there. Therefore in the vicinity of the focus the momentum components of the Hamiltonian trajectory $(\mathbf{x}(t,\mu), \mathbf{p}(t,\mu))$ are small. To leading order we can rewrite the Hamiltonian (8) in the form

$$H(\mathbf{x},\mathbf{p}) \approx H(\mathbf{q},\mathbf{p}) \equiv \mathbf{p}\hat{\mathbf{d}}\mathbf{q} + {}^1/_2\mathbf{p}\hat{\mathbf{Q}}\mathbf{p}, \quad \mathbf{q} \equiv \mathbf{x} - \mathbf{x}_f \tag{31}$$

where $\hat{\mathbf{d}}$ and $\hat{\mathbf{Q}}$ are 2×2 matrices,

$$d_{ij} \equiv \sum_{\mathbf{r}} r_i [\partial w(\mathbf{x},\mathbf{r})/\partial x_j]_{\mathbf{x}_f}, \quad Q_{ij} \equiv \sum_{\mathbf{r}} w(\mathbf{x}_f,\mathbf{r}) r_i r_j, \quad i,j = 1,2 \tag{32}$$

The approximate Hamiltonian $H(\mathbf{q},\mathbf{p})$ is quadratic in the dynamical variables of the system near the focus; in fact, it has a special structure in the sense that H does not contain second-order terms in the new coordinate $\mathbf{q}$ (which is the old coordinate $\mathbf{x}$, normalized in that it is measured from the focus $\mathbf{x}_f$).

B. Eigenvectors and Eigenvalues near the Focus. The Hamiltonian equations of motion that follow from (31) may be written in matrix form as

$$\begin{pmatrix} \dot{\mathbf{q}} \\ \dot{\mathbf{p}} \end{pmatrix} = \hat{\mathbf{T}} \begin{pmatrix} \mathbf{q} \\ \mathbf{p} \end{pmatrix}, \quad \hat{\mathbf{T}} \equiv \begin{pmatrix} \hat{\mathbf{d}} & \hat{\mathbf{Q}} \\ \mathbf{0} & -\hat{\mathbf{d}}^\dagger \end{pmatrix} \tag{33}$$

Here $\hat{\mathbf{T}}$ is a 4×4 matrix. It is significant that one of the four 2×2 blocks of this matrix is equal to 0. This is not a specific feature of a particular model, but a consequence of the general features of the dynamics of extreme fluctuational paths. As a result, the eigenvalues and eigenvectors of $\hat{\mathbf{T}}$ generically have certain special features.

Two eigenvalues $\lambda_{1,2}$ of the matrix $\hat{\mathbf{T}}$ coincide with the eigenvalues of the matrix $\hat{\mathbf{d}}$. The corresponding eigenvectors of $\hat{\mathbf{T}}$ have their momentum parts $\mathbf{p}^D_{1,2}$ equal to zero, whereas their coordinate parts $\mathbf{q}^D_{1,2}$ are the eigenvectors of the matrix $\hat{\mathbf{d}}$. A linear combination

$$\begin{pmatrix} \mathbf{q}^D(t) \\ \mathbf{0} \end{pmatrix} \equiv C_1^D \begin{pmatrix} \mathbf{q}_1 \\ \mathbf{0} \end{pmatrix} e^{\lambda_1 t} + C_2^D \begin{pmatrix} \mathbf{q}_2^D \\ \mathbf{0} \end{pmatrix} e^{\lambda_2 t} \tag{34}$$

$$\lambda_{1,2} = \eta \pm i\omega \equiv {}^1/_2 \mathrm{tr}\, \hat{\mathbf{d}} \pm i[\det \hat{\mathbf{d}} - {}^1/_4(\mathrm{tr}\, \hat{\mathbf{d}})^2]^{1/2}, \quad \eta, \omega > 0$$

$$\mathbf{q}_1^D = (\mathbf{q}_2^D)^*, \quad C_1^D = (C_2^D)^*$$

describes the evolution of the mean species concentration vector $\bar{\mathbf{q}} \equiv \bar{\mathbf{x}}(t) - \mathbf{x}_f$ on the $\mathbf{q}$-plane. The trajectories $\mathbf{q}^D(t)$ can be obtained from the deterministic equations (4) linearized in the vicinity of $\mathbf{x}_f$. They move away from the unstable focus, and accordingly η, the real part of the eigenvalues, is positive. To emphasize the "deterministic" nature of these trajectories and of the corresponding eigenvectors of the matrix $\hat{\mathbf{T}}$, we are using the superscript D.

The other two eigenvalues of the matrix $\hat{\mathbf{T}}$ (33), λ_3 and λ_4, are equal to $-\lambda_1$ and $-\lambda_2$, respectively. The corresponding "fluctuational" (in contrast to deterministic) eigenvectors have nonzero coordinate and momentum parts, $\mathbf{q}^F_{1,2}$ and $\mathbf{p}^F_{1,2}$; here we use the subscripts 1, 2, in combination with the superscript F, to enumerate these eigenvectors. Linear combinations

$$\begin{pmatrix} \mathbf{q}^F(t) \\ \mathbf{p}^F(t) \end{pmatrix} \equiv C_1^F \begin{pmatrix} \mathbf{q}_1^F \\ \mathbf{p}_1^F \end{pmatrix} e^{-\lambda_1 t} + C_2^F \begin{pmatrix} \mathbf{q}_2^F \\ \mathbf{p}_2^F \end{pmatrix} e^{-\lambda_2 t} \tag{35}$$

$$\mathbf{q}_1^D = (\mathbf{q}_2^D)^*, \quad C_1^F = (C_2^F)^*$$

are the solutions of (33) specific to the auxiliary system with the Hamiltonian (31). In contrast to the deterministic trajectories (34), the trajectories (35) approach the unstable focus $\mathbf{q} = \mathbf{0}$ as $t \to \infty$.

An arbitrary zero-energy classical trajectory, as determined by Hamilton's equations together with the Hamiltonian (31), is a linear superposition of the trajectories (34) and (35), i.e.,

$$\begin{pmatrix} \mathbf{q}(t) \\ \mathbf{p}(t) \end{pmatrix} = \begin{pmatrix} \mathbf{q}^D(t) + \mathbf{q}^F(t) \\ \mathbf{p}^F(t) \end{pmatrix} \tag{36}$$

C. Extreme Fluctuational Paths. We are interested in zero-energy classical trajectories of the form (36), which are extreme fluctuational paths, extended to the vicinity of the unstable focus. These paths emerge from the limit cycle and, as we have explained above, lie in the Lagrangian manifold of the limit cycle. According to eq 23 they form a one-parameter set, $(\mathbf{q}(t,\mu), \mathbf{p}(t,\mu))$ (where $\mathbf{q}(t,\mu) \equiv \mathbf{x}(t,\mu) - \mathbf{x}_f$). The parameter μ determines the values of the coefficients $C^{F,D}_{1,2}$ in eqs 34−36 for the paths on the LM. In general, to find this dependence, it is necessary to integrate eqs 15 with the initial conditions (23) from the vicinity of the limit cycle down to the range of small $|\mathbf{q}|$. We shall show, however, that the singular features of the pattern of extreme paths in the vicinity of an unstable focus in the chemical kinetics context can be found from a local analysis.

A key role in this analysis is played by the *most probable hitting path* (MPHP), along which the oscillating chemical system is most likely to move from the limit cycle to the unstable focus $\mathbf{q} = \mathbf{0}$, when Ω is large. The action for reaching the focus along (possibly, several) extreme trajectories is different; the MPHP is the trajectory for which this action is a minimum. We normalize our parametrization of extreme trajectories by setting the parameter μ to zero for the MPHP.

In general the Lagrangian manifold formed by the paths $(\mathbf{q}(t,\mu), \mathbf{p}(t,\mu))$ is locally smooth near the MPHP. This means that, for paths lying on the LM, the coefficients $C^F_{1,2}$, $C^D_{1,2}$ are smooth functions of μ for small $|\mu|$. In other words, at any given instant of time t the values of the coefficients $C^F_{1,2}$, $C^D_{1,2}$ for the extreme paths $\mathbf{q}(t,\mu)$, $\mathbf{p}(t,\mu)$ are close to the values of $C^F_{1,2}$, $C^D_{1,2}$ for the MPHP $(\mathbf{q}(t,0), \mathbf{p}(t,0))$ and can be found by expanding $C^F_{1,2}$, $C^D_{1,2}$ in a Taylor series in μ.

At $\mu = 0$ the coefficients $C^D_{1,2} = 0$ (otherwise the path would not go to the focus as $t \to \infty$, cf. (34)). On the other hand, the coefficients $C^F_{1,2}$ take on nonzero values at $\mu = 0$. By changing the time origin these coefficients can always be made equal to each other. Their value (denoted by κ in eq 37 below) can be found by integrating eqs 15 all the way down from the vicinity of the limit cycle. Then, with account taken of eqs 34 and 35, any extreme trajectories that lies on the Lagrangian manifold close to the MPHP can be written as a linear combination of the form

$$\begin{pmatrix}\mathbf{q}(t,\mu)\\ \mathbf{p}(t,\mu)\end{pmatrix} = \kappa \sum_{i=1,2} \begin{pmatrix}\mathbf{q}^F_i\\ \mathbf{p}^F_i\end{pmatrix} \exp[-\lambda_i t] + \mu \sum_{i=1,2} C^D_i \begin{pmatrix}\mathbf{q}^D_i\\ 0\end{pmatrix} \exp[\lambda_i t] \tag{37}$$

The first term in (37) corresponds to the MPHP. The terms $\propto \mu$ allow for admixture of the deterministic solution (34). In the derivative $\partial\mathbf{q}(t,\mu)/\partial\mu$ in (37) we have neglected the terms proportional to the fluctuational eigenvectors $\mathbf{q}^F_{1,2}$ and retained only those proportional to the deterministic eigenvectors $\mathbf{q}^D_{1,2}$. This could be done because the terms $\propto \mathbf{q}^F_{1,2}$ in (37) decay in time, whereas those $\propto \mathbf{q}^D_{1,2}$ increase exponentially with t. Therefore even if the terms $\mu\mathbf{q}^F_{1,2} \exp[-\lambda_{1,2}t]$ and $\mu\mathbf{q}^D_{1,2} \exp[\lambda_{1,2}t]$ were of the same order of magnitude at a certain instant $t = t_0$, when

$$\exp[(\lambda_1+\lambda_2)(t-t_0)] \gg 1$$

the former terms would be exponentially smaller than the latter.

By appropriately renormalizing μ one can always make the absolute value of the coefficients $C^D_{1,2}$ in (37) equal to 1. The phase of $C^D_{1,2}$ is determined by the normalization of the eigenvectors in (34) and (35). To choose the normalization, we notice first that $\mathbf{q}^D_i$ and $\mathbf{p}^F_{3-i}$ are eigenvectors of the matrices $\hat{\mathbf{d}}$ and $-\hat{\mathbf{d}}^\dagger$, respectively, and therefore they are orthogonal for $\lambda_1 \neq \lambda_2$, i.e.,

$$\mathbf{q}^D_i \cdot \mathbf{p}^F_{3-i} \equiv 0, \quad i = 1, 2 \tag{38}$$

It follows from the zero-energy condition, i.e., $H = 0$, that for any extreme trajectory there holds the identity

$$\lambda_1 \mathbf{q}^D_1 \cdot \mathbf{p}^F_1 C^D_1 + \lambda_2 \mathbf{q}^D_2 \cdot \mathbf{p}^F_2 C^D_2 = 0 \tag{39}$$

from which we have $|\mathbf{p}^F_2 \cdot \mathbf{q}^D_2| = |\mathbf{p}^F_1 \cdot \mathbf{q}^D_1|$.

The phases and lengths of the eigenvectors with superscripts D and F are independent of each other, and it is convenient for what follows to choose them so that

$$\mathbf{p}^F_2 \cdot \mathbf{q}^D_2 = \mathbf{q}^D_1 \wedge \mathbf{q}^D_2 = \mathrm{i}/2 \tag{40}$$

(respectively, $\mathbf{p}^F_1 \cdot \mathbf{q}^D_1 = -\mathrm{i}/2$). Here

$$\mathbf{A} \wedge \mathbf{B} \equiv A_1 B_2 - A_2 B_1$$

is the standard definition of the wedge product of two 2-vectors.

We have from (39)

$$C^D_2 = (C^D_1)^* = \mathrm{i}e^{-\mathrm{i}\phi}, \quad \phi = \arctan\frac{\eta}{\omega} \tag{41}$$

Equations 37 and 41 show that any extreme trajectory $\mathbf{q}(t,\mu)$ near the unstable focus can be viewed as a superposition of two spirals, $\mathbf{q}(t,0) = \mathbf{q}^F(t)$ and $\mu\partial\mathbf{q}/\partial\mu = \mathbf{q}^D(t)$. The spirals have equal-in-magnitude and opposite-in-sign decrements $\pm\eta$ and the same angular frequency ω and direction of rotation. The last is determined by the direction of the cross product of the velocity and the coordinate, or equivalently by the sign of the wedge product

$$\mathrm{sgn}\left(\frac{\mathrm{d}\mathbf{q}^D(t)}{\mathrm{d}t} \wedge \mathbf{q}^D(t)\right) = \mathrm{sgn}\left(\frac{\mathrm{d}\mathbf{q}^F(t)}{\mathrm{d}t} \wedge \mathbf{q}^F(t)\right) = \mathrm{sgn}\, d_{12} \tag{42}$$

Here we have taken into account that $d_{12}d_{21} < 0$ and that $d_{12}d_{21} + {}^1\!/_4(d_{11} - d_{22})^2 < 0$ for a focus, according to eq 34.

The MPHP corresponds to the converging spiral above, i.e., is an extreme trajectory with no admixture of the deterministic spiral. We note that the global parameter κ in (37) can always be chosen within an interval

$$\kappa_1 \exp(-2\pi\eta/\omega) \leq \kappa < \kappa_1$$

where κ_1 is arbitrary. The results should be independent of κ_1, and in what follows we assume that κ is of order unity.

Extreme trajectories of the form (37) with $|\mu| \ll 1$ spiral down to the unstable focus, remaining close to the MPHP (which has $\mu = 0$) up to the time when $t \approx (2\eta)^{-1}\ln|\mu|^{-1}$, or equivalently, until they reach a distance $\sim|\mu|^{1/2}$ from the focus. At that time, the second term in (37) becomes of the same order as the first term. At larger times, the deterministic term $\mu\partial\mathbf{q}/\partial\mu$ increasingly dominates. The extreme trajectories begin to wind back outward, and eventually approach deterministic trajectories of the form (34).

VI. Structure of the Lagrangian Manifold near an Unstable Focus

A. The Caustic in the Vicinity of an Unstable Focus. A remarkable feature of the flow field of extreme trajectories near an unstable focus is the presence of a caustic that spirals down to the focus. To show this, we note that a caustic is the envelope of a family of trajectories. In this case, it is an envelope of the parametrized set of paths $\mathbf{q}(t,\mu)$. So on a caustic, the one-to-one correspondence between the spatial coordinates (q_1, q_2) and the alternative coordinates (t, μ) is broken. That is, the Jacobian of the transformation from q_1, q_2 to t, μ is equal to zero.[12] This condition can be written in the form

$$\frac{\partial\mathbf{q}(t,\mu)}{\partial t} \wedge \frac{\partial\mathbf{q}(t,\mu)}{\partial\mu} = 0 \tag{43}$$

It can be shown from eqs 37, 39, and 40 that eq 43 always has a solution near an unstable focus. This means that a caustic is always present near an unstable focus except in the special (nongeneric) case when angular and radial fluctuations are decoupled (e.g., near a Hopf bifurcation point). In fact, we obtain from (43) that on the caustic

$$\mu = \mu_c(t) \equiv \frac{\kappa}{\cos\phi}\exp(-2\eta t)(\Gamma^{FD}_{12} \exp[-2i(\omega t + \phi)] - \Gamma^{FD}_{11}) + \text{c.c.} \tag{44}$$

and

$$\mathbf{q} = \mathbf{q}_c(t) \equiv \mathbf{q}(t,\mu_c(t)) \tag{45}$$

Here

$$\Gamma_{ij}^{FD} \equiv \mathbf{q}_i^F \wedge \mathbf{q}_j^D, \quad i,j = 1,2 \tag{46}$$

are the (oriented) areas spanned by the corresponding pairs of eigenvectors, as defined in the last section.

It follows from eqs 37, 44, and 45 that the caustic spirals down to the unstable focus. However, although the displacement vector $\mathbf{q}_c(t)$ is proportional to $\exp(-\eta t)$, the decay of $|\mathbf{q}_c(t)|$ as $t \to \infty$ will be nonmonotonic. In fact, $\mathbf{q}_c(t)$ will oscillate nonsinusoidally: since $\mu_c(t)$ is oscillating at the frequency 2ω, the function $\mathbf{q}_c(t)$ has terms that oscillate at frequencies ω and 3ω.

Using explicit expressions for the eigenvectors $\mathbf{q}_{1,2}^{F,D}$, which can be obtained from (33), and taking into account that the matrix $\hat{\mathbf{Q}}$ is nonnegative, one can show that

$$|\Gamma_{11}^{FD}| > |\Gamma_{21}^{FD}|\left[1 + \frac{\omega^2}{\eta^2}\right]^{1/2} \tag{47}$$

As a consequence, μ_c never becomes equal to zero. This means that the MPHP (the extreme trajectory with $\mu = 0$) touches the caustic at no point. Depending on the parameters of the system, the caustic may either be smooth or have cusp points, i.e., points where $\dot{\mathbf{q}}_c = 0$, lying along it.

The total number of irreducible parameters that characterize the dynamics of extreme paths near the focus turns out to be equal to 3. Although the Hamiltonian (31) contains two 2×2 matrices, one can make a linear (but not unitary) transformation,[32] which reduces the matrices $\hat{\mathbf{d}}$, $\hat{\mathbf{Q}}$ to the form

$$\hat{\mathbf{Q}}' = 2\begin{pmatrix} \eta - a & 0 \\ 0 & \eta + a \end{pmatrix}, \quad \hat{\mathbf{d}}' = \begin{pmatrix} \eta - a & b \\ -b & \eta + a \end{pmatrix} \tag{48}$$

$$b^2 = a^2 + \omega^2, \quad \eta > |a|$$

The only three parameters of the transformed Hamiltonian are then a, b, and η. (These parameters are not quite uniquely determined; the signs of a, b can be changed by changing the directions of the axes.) In the present and next sections we assume that $\eta > 3|a|$, in which case the caustic in the vicinity of the focus turns out not to have cusp points lying along it; that is, $\dot{\mathbf{q}}_c(t) \neq 0$ at all sufficiently large times t. One can show that in this case the velocity of any extreme trajectory is antiparallel to that of the caustic at the moment it is reflected from it, i.e.,

$$\dot{\mathbf{q}}_c(t)\cdot[\dot{\mathbf{q}}(t,\mu)]_{\mu=\mu_c(t)} < 0 \quad \text{if} \quad \eta > 3|a| \tag{49}$$

B. The Pattern of Extreme Trajectories in Polar Coordinates. The behavior of extreme paths near an unstable focus can easily be expressed in terms of polar coordinates $|q|$ and Θ defined by

$$q_1 = q\cos\Theta, \quad q_2 = q\sin\Theta \tag{50}$$

In what follows we define Θ as a running phase; it is allowed to vary continuously from $-\infty$ to ∞ along an extreme trajectory.

In polar coordinates, the focus is located at $q = 0$. It follows from eq 37 that, for the MPHP (the extreme trajectory with $\mu = 0$), the phase $\Theta \equiv \Theta_{MPHP}$ is a monotonic function of time: $\tan\Theta_{MPHP}$ is a linear function of $\tan\omega t$. By choosing the initial phase, one can put the phase Θ_{MPHP} and time t into one-to-one correspondence. Over a period $2\pi/\omega$ the phase Θ_{MPHP} is incremented by $2\pi\ \mathrm{sgn}\ d_{12}$, whereas the radius of the MPHP decreases by a factor $\exp[-2\pi\eta/\omega]$.

Extreme paths in polar coordinates are shown in Figure 2. Extreme paths to either side of the MPHP first move toward the origin $q = 0$, like the MPHP, but eventually go away from it. The caustic lies between the MPHP and the origin. This can be shown by investigating from which side the extreme paths touch the caustic, but it is also clear from the argument that the caustic goes toward the origin as $t \to \infty$, whereas extreme paths with $\mu \neq 0$ eventually go away from the origin. Therefore extreme paths lying between the MPHP and the origin should intersect the MPHP, which is possible provided they have encountered a caustic and have accordingly moved to another sheet of the Lagrangian manifold (cf. Figure 1). This argument does not merely show where the caustic is located: it also shows why a caustic should arise in the present problem.

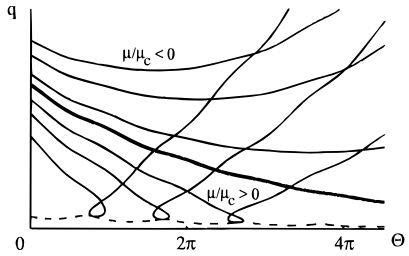

Figure 2. Extreme fluctuational trajectories near the unstable focus at $q = 0$, in polar coordinates (q, Θ). The bold line is the formally most probable hitting path (MPHP), along which fluctuations to the vicinity of the focus are most likely to occur for $\Omega \gg 1$. The dashed line indicates the position of a caustic, from which the extreme trajectories with $\mu/\mu_c > 0$ are reflected. This Figure is plotted in a frame in which linearized dynamics near the focus are specified by matrices of the form given in eqs 48, with parameters $a = 0.13$, $\omega = 3.5$, $\eta = 0.41$, and $b < 0$.

Along extreme trajectories that are very close to the MPHP ($|\mu| \exp(2\eta t) \ll 1$), the phase $\Theta(t,\mu)$ is monotonic as a function of time. It is also monotonic for extreme paths that have deviated far enough from the MPHP that the second (deterministic) term in (37) has become dominant (i.e., $|\mu| \exp(2\eta t) \gg 1$). In models with $\eta < 3|a|$, where the velocity of the caustic never becomes equal to 0, the phase of the caustic is monotonic as well. From this argument and from the fact that the velocity of an extreme trajectory and that of the caustic are oppositely directed at their point of tangency (cf. (49)), it follows that extreme paths that touch the caustic must be making *loops*. These loops are clearly seen in Figure 2. We note that the different parts of a loop lie on different sheets of the Lagrangian manifold (cf. Figure 1). Extreme paths on the same sheet of the LM are not self-intersecting and also cannot intersect one another.

C. Self-Similarity of the Lagrangian Manifold. The above analysis in terms of polar coordinates suggests that the Lagrangian manifold $\mathbf{p} = \mathbf{p}(\mathbf{q})$ near an unstable focus, as formed by the trajectories $(\mathbf{q}(t,\mu), \mathbf{p}(t,\mu))$ of (37), should be *self-similar*: it should be invariant with respect to a rotation of the coordinates by π and a simultaneous rescaling of variables. That is, it should be invariant under the transformation

$$\Theta \to \Theta - \pi n\ \mathrm{sgn}\ d_{12} \tag{51}$$

accompanied by a rescaling, i.e., under

$$\mathbf{q} \to (-1)^n \mathbf{q}\exp\left(-\frac{\pi n\eta}{\omega}\right), \quad \mathbf{p} \to (-1)^n \mathbf{p}\exp\left(-\frac{\pi n\eta}{\omega}\right) \tag{52}$$

The self-similarity can be verified as follows. It follows from (37) that at any instant t all points $\mathbf{q}(t,\mu)$ on the $\mathbf{q}$-plane lie on a straight line, with different points corresponding to different values of the parameter μ. The momentum at each point is the same and is equal to the momentum for the MPHP, $\mathbf{p}(t,0)$. Over half a period π/ω this straight line rotates around the point $\mathbf{q} = 0$ by the angle $\Theta = -\pi\ \mathrm{sgn}\ d_{12}$. As a result each point $\mathbf{q}(t,\mu)$

on the line goes over into another point on the same line, i.e.,

$$\mathbf{q}(t,\mu) \rightarrow \mathbf{q}(t+\pi/\omega,\mu e^{-2\pi\eta/\omega})$$

The only Hamiltonian trajectory on the LM that remains invariant under the transformation (52) is accordingly the MPHP (for which $\mu = 0$).

We shall now consider the cross section of the LM $\mathbf{p} = \mathbf{p}(\mathbf{q})$ by a given plane $q_2/q_1 = \text{const}$, i.e., a plane at a specified value of $\Theta(\text{mod } 2\pi)$. The first important feature seen in Figure 2 is that the LM has *infinitely many sheets*. These sheets correspond to values of the extended phase Θ that differ by 2π, i.e., to cross sections of the pattern in Figure 2 by vertical lines separated by $\delta\Theta = 2\pi$. All sheets of $\mathbf{p} = \mathbf{p}(\mathbf{q})$ are similar to each other, according to eq ([52): they can be obtained from one another by multiplying $\mathbf{p}$ and $\mathbf{q}$ by the factor $\exp(-2\pi n\eta/\omega)$. Therefore to obtain the global shape of the LM, it suffices to analyze a single sheet, which corresponds to a given Θ in Figure 2.

Extreme trajectories $\mathbf{q}(t,\mu)$ with the same Θ in Figure 2 differ in their values of μ and t. It is convenient to parametrize μ and q by t and Θ. From (37) we have

$$\mu(t;\Theta) = -\frac{\mathbf{q}(t,0) \wedge \hat{\mathbf{n}}(\Theta)}{[\partial\mathbf{q}(t,\mu)/\partial\mu] \wedge \hat{\mathbf{n}}(\Theta)}, \quad \hat{\mathbf{n}}(\Theta) \equiv (\cos\Theta, \sin\Theta) \tag{53}$$

($\hat{\mathbf{n}}(\Theta)$ is the unit vector that makes an angle $\Theta(\text{mod } 2\pi)$ with the q_1-axis of the $\mathbf{q}$-plane). Equation 53 describes, in parametric form, a branch of the momentum $\mathbf{p}$ for a given Θ in Figure 2, as a function of q. We note, again, that the value of the momentum is equal to that for the MPHP, i.e., $\mathbf{p} \equiv \mathbf{p}(t(q,\Theta),0)$. The projection of the momentum component p_1 as a function of the coordinate q is shown in Figure 3 at two values of Θ that differ by 2π and hence correspond to one and the same half-plane $q_2/q_1 = \tan\Theta$.

A generic feature of the many-branched function $p_1 = p_1(q)$ that can be seen in Figure 3 is that each continuous branch is two-valued; that is, it corresponds to two sheets of the LM. This is a consequence of the presence of the caustic. It was explained above that caustics correspond to folds of the LM (cf. Figure 1). The point where $|dp_1/dq| \rightarrow \infty$ is the cross section of the fold in the surface $p_1(\mathbf{q})$ by the half-plane $\mathbf{q}\cdot\hat{\mathbf{n}}(\Theta) = \text{const}$.

To complete the qualitative picture of the behavior of $p_1 = p_1(q)$, we note that, for a given Θ in Figure 2, large values of q (compared to the value of q on the MPHP for $\Theta_{\text{MPHP}} = \Theta$) correspond to large $|\mu| \exp(2\eta t)$ in eq 37; that is, such q are given by the deterministic term $\mu[C_1^D \mathbf{q}_1^D \exp[(\eta+i\omega)t] + \text{c.c.}]$ in eq 37. In Figure 2 there are two paths that arrive at a given large q at a given Θ, one with $\mu > 0$ and one with $\mu < 0$. Since the value of the coordinate $\mathbf{q}$ is the same for both paths, it is clear that the arguments ωt of the terms with opposite-sign μ differ by π; that is, the values of t differ by π/ω. (This can also be shown using (37).) The momenta $\mathbf{p}(t,\mu) \equiv \mathbf{p}(t,0)$ are equal in magnitude and opposite in sign for the two paths. This means that, for large q, the function $p_1 = p_1(q)$ takes on a pair of values that are of equal magnitude and opposite sign, as shown in Figure 3.

We may also note that, for large values of q at each μ, the phase Θ is given by the ratio of the components of the vector $\mu[C_1^D \mathbf{q}_1^D \exp[(\eta+i\omega)t] + \text{c.c.}]$. It is independent of the sign of μ and is determined only by the time t. Therefore the value of t is the same at points with a given Θ but different values for the parameter μ (and hence different values for q). As a consequence of this, the function $p_1 = p_1(q)$ reduces to a constant when q, the displacement from the unstable focus, is large.

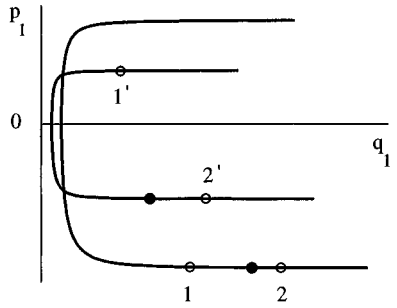

Figure 3. Cross section of the self-similar helicoidal surface $p_1 = p_1(\mathbf{q})$ by the half-plane $q_2 = 0$, $q_1 > 0$. Two successive branches, corresponding to $\Theta = 2\pi n$ and $\Theta = 2\pi(n+1)$, with n an integer, are shown. The coordinate frame and model parameters are the same as in Figure 2. The filled circles indicate successive positions (intersection points, actually) of the MPHP. They lie on a straight line that passes through the point $(\mathbf{q}, \mathbf{p}) = (\mathbf{0}, \mathbf{0})$. The open circles indicate intersection points of two extreme trajectories other than the MPHP. Over a turn around the focus, trajectory 1 (with $\mu/\mu_c > 0$) passes over the fold in the surface and goes from the lower to the upper sheet of $p_1(q,\Theta)$. Trajectory 2 has $\mu/\mu_c < 0$; it stays on the side opposite the caustic with respect to the MPHP (cf. Figure 2).

D. Extreme Trajectories on the LM. The total number of sheets of the Lagrangian manifold $\mathbf{p} = \mathbf{p}(\mathbf{q})$ is infinite, since each sheet is a "reduced copy" of the former one (formed by extreme trajectories with t reduced by $2\pi/\omega$). Successive sheets are nested into one another, as seen in Figure 3. The manifold as a whole has a helicoidal, whorl-type shape. The fold of the LM spirals down to the unstable focus $(\mathbf{q}, \mathbf{p}) = (\mathbf{0}, \mathbf{0})$. Far from the small-$\mathbf{q}$ range, in regions of the species concentration space where the linear theory developed above does not apply, the different branches of $\mathbf{p} = \mathbf{p}(\mathbf{q})$ turn out to be connected to each other. That is, the Lagrangian manifold is globally connected, though it does not appear to be connected in the linear approximation.

Figure 3 gives insight into the behavior of the Hamiltonian trajectories $(\mathbf{q}(t,\mu), \mathbf{p}(t,\mu))$, which form the LM. Each trajectory corresponds to a point (q, p_1) on a branch $p_1 = p_1(q)$, and the positions of the points on successive branches show how the trajectory is changed over the time period $2\pi/\omega$.

The behavior of the MPHP is of special interest. We note that the MPHP is a *heteroclinic trajectory* in the four-dimensional phase space; it extends from the limit cycle to the focus and in fact lies both in the LM (which is the unstable manifold of the limit cycle) and in the stable manifold of the focus. The latter is traced out by the family of trajectories $(\mathbf{q}^F(t), \mathbf{p}^F(t))$ of the form (35) and is seen from (35) to be a plane $\mathbf{p} = \hat{\mathbf{A}}\mathbf{q}$ in the immediate vicinity of the focus. As a consequence, successive projections of the MPHP on $p_1(q)$ lie on a straight line, as would be expected also from eq 37.

Extreme trajectories with μ of opposite sign deviate from the MPHP in opposite directions (cf. Figure 2). Trajectories with $\mu/\mu_c < 0$ approach the fold of the LM, and their projections (p_1, q) approach the singularity of the LM cross section $p_1(q)$, where $|dp_1/dq| \rightarrow \infty$. Subsequently they go over the fold and come to the other sheet of the same branch of $p_1 = p_1(q)$. It follows from eq 44 that each extreme trajectory goes over a fold only once.

Extreme trajectories with $\mu/\mu_c > 0$, on the other hand, move away from the MPHP toward larger values of q, as do the points (p_1, q) in Figure 3 that arise from such trajectories. Such trajectories never encounter the fold in the LM. Nonetheless their projections on the $\mathbf{q}$-plane are self-intersecting and intersect projections of other trajectories. This is an interesting feature of the topology of the LM. In general, infinitely many trajectories on the LM, when projected onto the $\mathbf{q}$-plane, pass through any point.

VII. The Action and the Switching Line

The expression for the action, eq 25, in combination with the explicit expressions for the extreme trajectories in the vicinity of the unstable focus, i.e., (34)−(37), makes it possible to evaluate the action near the focus explicitly, as

$$S(t,\mu) \approx S_{\rm f} + \mu \mathbf{p}(t,0)\cdot\left[\frac{\partial \mathbf{q}(t,\mu)}{\partial \mu}\right]_{\mu=0} - \int_t^{\infty} \mathbf{p}(\tau,0)\cdot\mathbf{q}(\tau,0)\,{\rm d}\tau \tag{54}$$

where $S_{\rm f}$ is the action at the focus itself. In deriving (54) we have used the approximation

$$S(t,\mu) \approx S(t,0) + \mu \mathbf{p}(\mathbf{t},\mu)\cdot\left[\frac{\partial \mathbf{q}(t,\mu)}{\partial \mu}\right]_{\mu=0}$$

which is valid at small $|\mu|$.

Using eqs 37−41 and 46, we further obtain

$$S(t,\mu) = S_{\rm f} - \kappa\mu\cos\phi - \kappa^2 \sum_{i,j=1,2} \Gamma^{FD}_{j,3-i}\left(\frac{\lambda j}{\lambda_i + \lambda_j}\right){\rm e}^{-(\lambda_i+\lambda_j)t} \tag{55}$$

The classical action function $S = S(t,\mu)$ as given by (55) is single-valued. However, the action as a function of the species concentration vector $\mathbf{q}$ is in general multivalued, since extreme trajectories $\mathbf{q}(t,\mu)$ with different t, μ may cross each other. As a consequence, extreme trajectories with different values of the parameter μ may extend from the limit cycle to a point $\mathbf{q}$.

The form of the action S as a function of $\mathbf{q}$ can be evaluated directly from eqs 37 and 55, but insight into it can be gained from Figure 3. Since all extreme trajectories have zero energy, we necessarily have[25]

$$S(\mathbf{q}) = \int \mathbf{p}\cdot{\rm d}\mathbf{q} \tag{56}$$

the line integral being taken along an extreme trajectory extending from the limit cycle to $\mathbf{q}$. (As noted, this trajectory may not be unique!) One can use ([56) to compute the cross section of the action surface $S = S(\mathbf{q})$ by a half-plane Θ(mod 2π) = const, from $\mathbf{p}\cdot\hat{\mathbf{n}}(\Theta)$, the momentum component in the direction $\hat{\mathbf{n}}(\Theta)$. The form of $\mathbf{p}\cdot\hat{\mathbf{n}}(\Theta)$ as a function of the radial coordinate q is similar to that of $p_1(q)$ displayed in Figure 3 (in fact if $\Theta = 2\pi n$ in Figure 3, then $\mathbf{p}\cdot\hat{\mathbf{n}}(\Theta)$). Each branch of the momentum component in Figure 3 accordingly corresponds to a branch of the action S, which is obtained by integrating $\mathbf{p}\cdot\hat{\mathbf{n}}(\Theta)$.

A cross section of the action surface $S = S(\mathbf{q})$ is displayed in Figure 4. As would be expected from Figure 3 and eq 56, each branch of the action cross section contains a cusp point. Each such cusp point is attributable to the fold of the LM (since at it, $|{\rm d}[\mathbf{p}\cdot\hat{\mathbf{n}}(\Theta)]/{\rm d}q| \to \infty$). Away from cusp points, the two sheets of each branch of the cross section of S are nearly linear in q and have opposite slopes (since the values of $\mathbf{p}\cdot\hat{\mathbf{n}}(\Theta)$ are nearly q-independent, and have opposite signs). Different branches of S intersect each other.

As we explained in section IV A, only the minimum action at any point, $S_{\rm min}(\mathbf{q})$, is of physical interest, since it is the minimum action that appears in the eikonal approximation to the stationary probability density. The shape of the surface of minimum action is clear from Figure 4.

A. Self-Similarity of the Switching Line. Generically there is a single *dominant* extreme trajectory (by definition, the optimal fluctuational trajectory) that extends from the limit cycle to a given point $\mathbf{q}$ in the species concentration space. It is this trajectory that provides the value of the minimum action function, $S_{\rm min}(\mathbf{q})$. Areas of the q-plane reached via different sets of optimal trajectories are separated from one other by

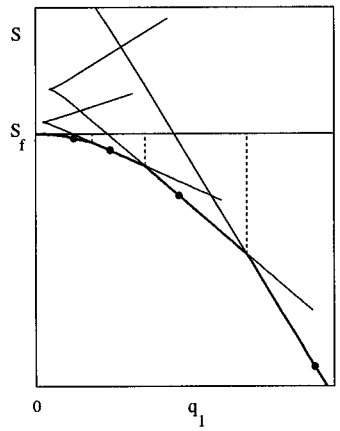

Figure 4. Cross section of the action surface $S = S(q_1,q_2)$ near the focus ($\mathbf{q} = \mathbf{0}$), by the half-plane $q_2 = 0$, $q_1 > 0$. The coordinate frame and model parameters are the same as in Figure 2, and the bold dots are placed at the points where the MPHP intersects the half-plane. The branches of S correspond to values of Θ that differ by 2π. The minimum action curve, $S_{\rm min} = S_{\rm min}(q_1,0)$, is indicated in bold; it is only piecewise smooth. The light dashed lines indicate points where the switching line intersects the q_1-axis; by definition, this occurs at points on the axis where branches intersect, and $S_{\rm min}$ is nondifferentiable.

switching lines. This means that, for optimal trajectories $\mathbf{q}(t,\mu)$ on one side of a switching line, the values of the parameter μ lie in one range, whereas for optimal trajectories terminating at points on the other side of the switching line, the range of values of μ is totally different. μ jumps discontinuously when the switching line is crossed.

The presence of a switching line is clearly indicated in Figure 4: its cross section is the series of points where successive branches of the cross section of S intersect one another.

The structure of the switching line can be understood if one takes into account the fact that the MPHP is (i) the optimal path that extends from the limit cycle to the unstable focus and (ii) a spiral. It follows from (i) that points $\mathbf{q}$ close to the MPHP are reached via optimal paths close to the MPHP and lying either inside or outside the MPHP spiral, depending on the choice of $\mathbf{q}$. On the other hand, when one moves transverse to the MPHP, one goes from the vicinity of one turn of the spiral to the vicinity of the next turn. Somewhere in between, switching should occur. The condition for this is that the actions for the two competing extreme trajectories terminating at a point $\mathbf{q}$ be equal to each other (cf. (28)), i.e.,

$$\mathbf{q}(t_1,\mu_1) = \mathbf{q}(t_2,\mu_2), \quad S(t_1,\mu_1) = S(t_2,\mu_2) \tag{57}$$

It can be immediately verified from the above equations that the switching line is self-similar: the transformation $\mathbf{q} \to (-1)^n\mathbf{q}\exp(-\pi n\eta/\omega)$ maps it onto itself, as it corresponds to the change of parameters

$$t_i \to t_i + \pi n/\omega, \quad \mu_i \to \mu_i \exp(-2\pi n\eta/\omega), \quad i = 1, 2$$

The switching line determined by eqs 37, 55, and 57 is shown in Figure 5. It is plotted in polar coordinates. In these coordinates, the points with the same q and with the values of Θ that differ by 2π correspond to the same point on the $\mathbf{q}$-plane. It is seen from Figure 2 that such points are reached along the trajectories that lie below and above the MPHP, the point with the value of Θ larger by 2π being reached along the upper trajectory. Therefore there should occur switching between the trajectories above and below the MPHP. The switching line (which is a single line on the $\mathbf{q}$-plane) is periodically repeating itself in polar coordinates, with the period 2π along the Θ -axis, as shown in Figure 5 (the MPHP is repeating itself as well). The lower and upper trajectories that arrive at the same $\mathbf{q}$ end

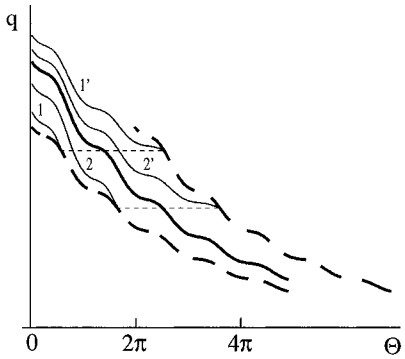

Figure 5. Optimal fluctuational paths near the unstable focus $\mathbf{q} = \mathbf{0}$, in a model with parameter values $a = 0.33$, $\omega = 4.1$, and $\eta = 0.45$. The plot is in terms of polar coordinates (q, Θ). The bold curve is the most probable hitting path (MPHP), which extends down to $q = 0$ as $\Theta \to \infty$. The bold dashed curve is the switching line (the two switching lines shifted by 2π along the Θ-axis correspond to one and the same switching line on the **q**-plane). When an extreme fluctuational trajectory reaches the switching line, it ceases to be optimal. Optimality passes from it to another extreme fluctuational trajectory, with Θ shifted by 2π. The light dashed lines indicate the way in which this process occurs.

up on the "replicas" of the switching line, which are shifted by 2π. The switching line spirals down to the unstable focus $\mathbf{q} = \mathbf{0}$ along with the MPHP and with the caustic (not shown in Figure 5), and these spirals nowhere intersect one another.

VIII. Extreme Trajectories for a Selkov Model

In this section we shall investigate numerically the pattern of extreme trajectories, including optimal fluctuational trajectories, in an oscillating, spatially homogeneous Selkov model. This model is described by the chemical reaction scheme

$$A \underset{k_2}{\overset{k_1}{\rightleftharpoons}} X_1, \quad X_1 + 2X_2 \underset{k_4}{\overset{k_3}{\rightleftharpoons}} 3X_2, \quad X_2 \underset{k_6}{\overset{k_5}{\rightleftharpoons}} B \tag{58}$$

The number of molecules of species A and B are held constant, while X_1 and X_2, the number of molecules of the two intermediate chemical species, can vary in time. The equations of motion for the average concentrations $\bar{x}_1$, $\bar{x}_2$ of the intermediate species have the form

$$\dot{\bar{x}}_1 = k_1 A/\Omega + k_4 \bar{x}_2^{\,3} - (k_2 + k_3 \bar{x}_2^{\,2})\bar{x}_1 \tag{59}$$

$$\dot{\bar{x}}_2 = k_6 B/\Omega + k_3 \bar{x}_2^{\,2} \bar{x}_1 - (k_5 + k_4 \bar{x}_2^{\,2})\bar{x}_2$$

(Recall that we are working in a volume of size Ω.) We shall set $k_1 A/\Omega = 2.0$, $k_2 = 0.34$, $k_3 = 1.4$, $k_4 = 0.02$, $k_5 = 2.2$, and $k_6 B/\Omega = 0.24$. With these parameter values, the two-dimensional dynamical system specified by eqs 59 has a stable limit cycle. In chemical terms, it models an oscillating reaction. There is an unstable focus located within the limit cycle, at the point $(x_{1f}, x_{2f}) \approx (1.83, 0.74)$.

The reduced transition rates $w(\mathbf{x},\mathbf{r})$ for reaction 58, as defined in (2), are nonzero for $(r_1, r_2) = (1, 0)$, $(-1, 0)$, $(-1, 1)$, $(1, -1)$, $(0, -1)$, or $(0, 1)$. These values of $\mathbf{r}$ correspond to the six possible reactions; for example, for $\mathbf{r} = (-1, 1)$ we have $w(\mathbf{x},(-1,1)) = k_3 x_1 x_2^{\,2}$.

We have analyzed the pattern of extreme trajectories for the Selkov model (58) by numerically integrating Hamilton's equations (eqs 15), equipped with the initial conditions of eq 23. A family of trajectories was obtained by varying the initial distance from the limit cycle at a certain point on the cycle. This parameter (initial distance from the limit cycle, denoted $\xi_2^{(0)}$ in section IIIB) is essentially the same as the trajectory-indexing parameter μ used in the previous sections.

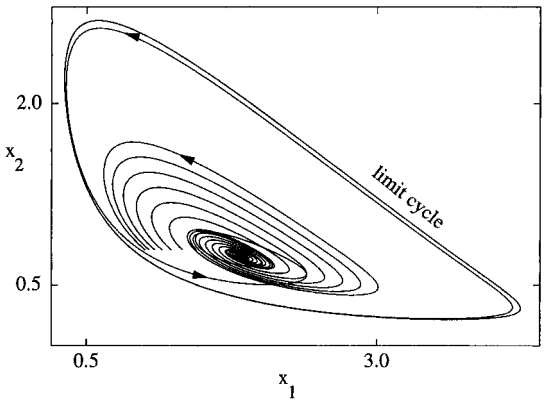

Figure 6. Tube of extreme fluctuational trajectories for the Selkov model ([REF:selkov]), projected to the species concentration plane. Parameters of the model are given in the text. The tube is very narrow near the limit cycle: separate trajectories are not resolved. Near the unstable focus, after several turns, trajectories other than the MPHP diverge from one another and spiral away. The arrows show the direction of motion.

A low-resolution plot is displayed in Figure 6. Near the limit cycle the extreme trajectories first go away from the cycle, forming a small-step spiral. We show an initially narrow tube of extreme paths (separate paths in the tube cannot be resolved visually near the cycle) as it spirals down to the unstable focus. Starting at a certain distance from the cycle, the step of the spiral dramatically increases, and the tube approaches the vicinity of the focus within a few turns. Near the focus the width of the tube sharply increases, and the trajectories in the tube diverge from one another and begin to move away from the focus. The only extreme trajectory that spirals down all the way to the focus is the MPHP (the formally most probable hitting path, in the limit $\Omega \to \infty$).

The behavior of the tube at a larger resolution is shown in Figure 7a,b. In Figure 7a one sees how the width of the tube varies as the trajectories spiral down toward the focus. When they are sufficiently close to the focus, the tube in Figure 7a splits into two parts. In both parts, the extreme trajectories make loops. This behavior is generic for one group of extreme trajectories near the focus, cf. Figure 2 (trajectories that lie on the opposite side of the MPHP with respect to those in Figure 7 eventually spiral away from the focus without making loops). The loops, at higher resolution, are shown in Figure 7b.

The envelopes of the loops made by extreme paths are caustics. The global structure of caustics is shown in Figure 8a,b. As we noted in section VIA, locating caustics numerically is facilitated by the fact that the Jacobian $J \equiv |\partial(q_1,q_2)/\partial(t,\mu)|$ vanishes at the time t when the extreme trajectory with parameter μ impinges on, and is reflected by, a caustic.[12] It is not difficult to show that as a function of t, the Jacobian satisfies a first-order differential equation along the extreme trajectory (cf. ref 9). In hunting for caustics we took into account only "primary" caustics, i.e., caustics that are encountered by extreme trajectories for the first time (caustics that are encountered by extreme trajectories that have already encountered a caustic are of no physical interest, since by that time, the extreme trajectories have ceased to be optimal).

As is shown in Figure 8a, two primary caustics start at a cusp point located midway between the limit cycle and the unstable focus (the point C). One caustic spirals down to the focus and the other spirals away from it. The caustic that spirals down to the focus is not smooth; it has an infinite number of cusp points lying along it, in the vicinity of the focus (see Figure 8b). These cusp points are well separated from the "initial" cusp, which lies far away from the focus. The presence of cusp points in the flow field of extreme trajectories is clear from

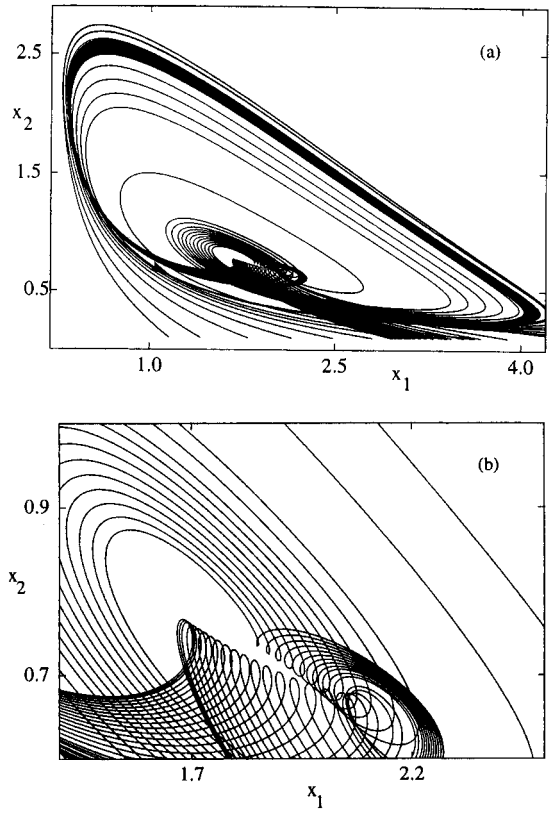

Figure 7. Plot implying the presence of a caustic in the flow field of extreme fluctuational trajectories in the Selkov model. (a) Tube of trajectories that emanate from the limit cycle (the tube is different from that shown in Figure 6). Near the unstable focus the trajectories make loops, are reflected from a caustic, and then spiral away from the focus. (b) Higher resolution plot of the same tube of extreme trajectories.

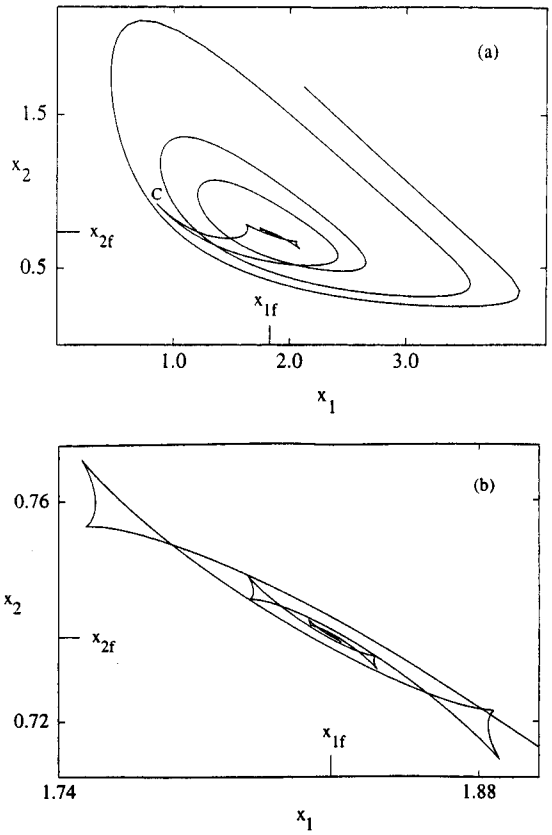

Figure 8. Location of the caustics in the flow field of extreme fluctuational trajectories in the Selkov model. (a) Two caustics that emerge from a cusp point, *C*. One of the caustics eventually spirals into the limit cycle; the other spirals down to the unstable focus. (b) High-resolution plot, showing the immediate vicinity of the unstable focus. The caustic is seen to be self-similar and to have, lying along its extent, infinitely many additional cusp points.

Figure 7b: cusps are located at points where caustics (the envelopes of the loops) merge together.

The difference between the shapes of the caustics shown in Figure 8a and the shape obtained analytically in section VI arises from the fact that for the parameter values we have chosen for the Selkov model we have $\eta \approx 0.22$ and $a \approx 0.17$. Here the parameters η and a, which determine the dynamics of fluctuational trajectories that extend to the vicinity of the unstable focus, are defined in terms of the linearized dynamics near the focus by eqs 48. As a consequence, the condition $\eta > 3|a|$ we assumed in section VI is violated. But analysis of the case $\eta > 3|a|$ is quite similar to that given in sections V−VII and will be presented elsewhere.[32] It follows from the results of such an analysis that, in models with $\eta > 3|a|$, the caustic still spirals down to the focus, but rather than being smooth, it contains four cusp points per turn.

IX. Conclusions

In this paper we have indicated how techniques of asymptotic analysis may be applied to yield results on the fluctuational behavior of oscillating chemical systems. The fluctuations we have considered are fluctuations away from a limit cycle in a space of species concentrations. The stationary probability distribution for an oscillating system in such a space is built up by fluctuations of this sort, and in the limit when Ω (a measure of volume, or total number of molecules) tends to infinity, the stationary distribution will be increasingly concentrated near the limit cycle. The tail of the stationary probability distribution, far from the limit cycle, is built up by large fluctuations. We have investigated the distribution both close to and far from the limit cycle.

We have also considered the pattern of optimal fluctuational trajectories, i.e., the most likely routes for fluctuational motion of the species concentration vector $\mathbf{x}(t)$ toward a specified point in the space of species concentrations, that is remote from the limit cycle. In the limit $\Omega \rightarrow \infty$, in which large fluctuations are exponentially rare, there normally exists a unique optimal (i.e., most probable) fluctuational path terminating at any specified point not on the limit cycle. The computation of such optimal trajectories is best accomplished through the analysis of an auxiliary Hamiltonian dynamical system. The "extreme" trajectories of this system, which are really zero-energy trajectories that move through its phase space, have optimal fluctuational trajectories as their projections on the space of the species concentrations **x**. Extreme trajectories are easily computed numerically; they trace out a so-called Lagrangian manifold in the phase space of the auxiliary system.

The flow field of optimal fluctuational trajectories normally displays a pattern of singularities that is different from the pattern of singularities appearing in the flow field of extreme trajectories arising in the semiclassical (WKB) computation of quantum-mechanical wave functions. In particular, optimal fluctuational trajectories never encounter caustics. (Strictly speaking, they may encounter them, but by the time they do so, they have ceased to be optimal.) However, the flow field of optimal trajectories in the space of species concentrations contains *switching lines*: curves separating regions that are reached, in the $\Omega \rightarrow \infty$ limit, via topologically different sorts of fluctuational paths.

Transverse to the limit cycle, the stationary probability density of the system is approximately Gaussian, with variance proportional to Ω^{-1}. But we have seen that if an unstable focus is contained within the limit cycle, behavior of the stationary probability density close to the unstable focus is more compli-

cated. One might think that it would be given, to a good approximation, by an inverted Gaussian. But we have analyzed the eikonal approximation $P_{st}(\mathbf{x}) \approx c(\mathbf{x}) \exp[-\Omega S(\mathbf{x})]$ to the stationary probability density P_{st} and have shown that normally the "action" function S is quite singular near an unstable focus. In particular, a switching line spirals down to any such focus, in a self-similar way: successive turns of the switching line are reduced copies of each other. And the gradient of S is discontinuous along a switching line.

We have compared the results of our theoretical analysis with detailed numerical results on the pattern of optimal fluctuational paths in an oscillating, homogeneous Selkov model. Numerical analysis of such a model is not difficult, and it demonstrates the occurrence of topological singularities we have predicted. Switching lines, in a flow field of optimal fluctuational trajectories, have recently been observed in noise-perturbed continuous dynamical systems.[6] Oscillating chemical systems that are mesoscopic rather than macroscopic, so that Ω is not so large as to suppress too greatly large fluctuations away from the limit cycle, surely merit experimental investigation: it is possible that a pattern of switching lines can be observed in such systems.

Acknowledgment. We are grateful to P. M. Hunt, who participated in this work at an early stage. We also acknowledge valuable discussions with K. L. C. Hunt and J. Ross. M.S. is grateful to the REU program at Michigan State University for financial support. The research of R.S.M. was partially supported by the National Science Foundation under Grant DMS-95-00792.

References and Notes

(1) Epstein, I. R. *J. Phys. Chem.* **1984**, *88*, 187.

(2) Hunt, K. L. C.; Hunt, P. M.; Ross, J. *Annu. Rev. Phys. Chem.* **1990**, *41*, 409.

(3) Westerhoff, H. V.; Chen, Y. *Proc. Natl. Acad. Sci.* **1985**, *82*, 3222.

(4) Blumenfeld, L. A.; Grosberg, A. Yu.; Tikhonov, A. N. *J. Chem. Phys.* **1991**, *95*, 7541.

(5) Vance, W.; Ross, J. *J. Phys. Chem.* **1995**, *103*, 2472.

(6) (a) Dykman, M. I.; McClintock, P. V. E.; Smelyanskiy, V. N.; Stein, N. D.; Stocks, N. G. *Phys. Rev. Lett.* **1992**, *68*, 2718. (b) Dykman, M. I.; Luchinsky, D. G.; McClintock, P. V. E.; Smelyanskiy, V. N. Submitted for publication.

(7) Hunt, K. L. C.; Hunt, P. M.; Ross, J. *J. Chem. Phys.* **1990**, *92*, 2572; **1991**, *96*, 618.

(8) Jauslin, H. R. *J. Stat. Phys.* **1986**, *42*, 573; *Physica* **1987**, *144A*, 179.

(9) Maier, R. S.; Stein, D. L. *Phys. Rev. Lett.* **1992**, *69*, 3691; *Phys. Rev. Lett.* **1993**, *71*, 1783; *Phys. Rev. E* **1993**, *48*, 931; *J. Stat. Phys.* **1996**, *83*, 291.

(10) Chinarov, V. A.; Dykman, M. I.; Smelyanskiy, V. N. *Phys. Rev. E* **1993**, *47*, 2448.

(11) Dykman, M. I.; Mori, E.; Ross, J.; Hunt, P. M. *J. Chem. Phys.* **1994**, *100*, 5735.

(12) Berry, M. V. *Adv. Phys.* **1976**, *35*, 1. Schulman, L. S. *Techniques and Applications of Path Integration*; Wiley: New York, 1981. Maslov, V. P.; Fedoriuk, M. V. *Semi-Classical Approximation in Quantum Mechanics*; Reidel: Boston/Dordrecht, 1981. Delos, J. B. *Adv. Chem. Phys.* **1986**, *65*, 161. Littlejohn, R. G. *J. Stat. Phys.* **1992**, *68*, 7.

(13) (a) Haken, H. *Synergetics: An Introduction*, 2nd ed.; Springer-Verlag: New York/Berlin, 1978. (b) van Kampen, N. G. *Stochastic Processes in Physics and Chemistry*; North-Holland: New York/Amsterdam, 1981.

(14) Gardiner, G. W. *Handbook of Stochastic Methods*, 2nd ed.; Springer-Verlag: New York/Berlin, 1990.

(15) Lax, M. In *Statistical Physics, Phase Transitions and Superconductivity*; Chrétien, M., Gross, E. P., Deser, S., Eds.; Gordon and Breach, New York, 1968.

(16) Dykman, M. I.; Chu, X.; Ross, J. *Phys. Rev. E* **1993**, *48*, 1646; **1995**, *52*, 6916.

(17) Nicolis, G.; Turner, J. W. *Physica A* **1977**, *89*, 326. Nicolis, G.; Malek-Mansour, M. *Prog. Theor. Phys. Suppl.* **1978** *64*, 249. Fraikin, A.; Lemarchand, H. *J. Stat. Phys.* **1985**, *41*, 531.

(18) Kubo, R.; Matsuo, K.; Kitahara, K. *J. Stat. Phys.* **1973**, *9*, 51. Kitahara, K. *Adv. Chem. Phys.* **1973**, *29*, 85.

(19) Wentzell, A. D. *Theory Probab. Its Appl.* **1976** *21*, 227, 499. Maier, R. S. *Random Struct. Algorithms* **1991** *2*, 379; In *1992 Lectures on Complex Systems*; Addison-Wesley: New York, 1993.

(20) Matkowsky, B. J.; Schuss, Z.; Knessl, C.; Tier, C; Mangel, M. *Phys. Rev. A* **1984**, *29*, 3359. Knessl, C.; Mangel, M.; Matkowsky, B. J.; Schuss, Z.; Tier, C. *J. Chem. Phys.* **1984**, *81*, 1285. Knessl, C.; Matkowsky, B. J.; Schuss, Z. *J. Stat. Phys.* **1986**, *42*, 169.

(21) Hu Gang, *Z. Phys. B* **1986**, *65*, 103; *Phys. Rev. A* **1987**, *36*, 5782.

(22) Vlad, M.; Ross, J. *J. Chem. Phys.* **1994**, *100*, 7268; **1994**, *100*, 7279; **1994**, *100*, 7295.

(23) Naeh, T.; Kłosek, M. M.; Matkowsky, B. J.; Schuss, Z. *SIAM J. Appl. Math.* **1990**, *50*, 595.

(24) Wentzell, A. D.; Freidlin, M. I. *Russ. Math. Surveys* **1970** *25*, 1. Freidlin, M. I.; Wentzell, A. D. *Random Perturbations in Dynamical Systems*; Springer-Verlag: New York/Berlin, 1984.

(25) Landau, L. D.; Lifshitz, E. M. *Mechanics*; Pergamon: London, 1976.

(26) Ludwig, D. *SIAM Rev.* **1975**, *17*, 605.

(27) Dykman, M. I.; Krivoglaz, M. A. *Soviet Phys. JETP* **1979**, *50*, 30.

(28) Graham, R.; Tél, T. *Phys. Rev. Lett.* **1984**, *52*, 9. Graham, R.; Tél, T. *J. Stat. Phys. 35*, 729. Graham, R.; Tél, T. *Phys. Rev. A* **1985**, *31*, 1109.

(29) Dykman, M. I.; Millonas, M. M.; Smelyanskiy, V. N. *Phys. Lett. A* **1994**, *195*, 53.

(30) Arnold, V. I. *Mathematical Methods of Classical Mechanics*; Springer-Verlag: New York/Berlin, 1978.

(31) Guckenheimer, J.; Holmes, P. *Nonlinear Oscillators, Dynamical Systems and Bifurcations of Vector Fields*; Springer-Verlag: New York/Berlin, 1983.

(32) Smelyanskiy, V. N.; Dykman, M. I.; Maier, R. S. In preparation.

(33) Whitney, H. *Ann. Math.* **1955**, *62*, 374. Arnold, V. I. *Catastrophe Theory*; Springer-Verlag: New York/Berlin, 1984.

JP962746I